**Tungsten chalcogenides as anodes for potassium-ion batteries**

Yuhan Wu[1,2,*], Weihao Xia[3], Yunzhuo Liu[3], Pengfei Wang[1], Yuhang Zhang[1], Jinru Huang[3], Yang Xu[4], Deping Li[3,*], Lijie Ci[3,*]

[1]School of Environmental and Chemical Engineering, Shenyang University of Technology, Shenyang 110870, China

[2]Key Laboratory of Advanced Energy Materials Chemistry (Ministry of Education), Nankai University, Tianjin 300071, China

[3]State Key Laboratory of Advanced Welding and Joining, School of Materials Science and Engineering, Harbin Institute of Technology (Shenzhen), Shenzhen, 518055, China

[4]Department of Chemistry, University College London, London WC1H 0AJ, UK

Corresponding Author:

E-mail:

yuhanwu@sut.edu.cn (Yuhan Wu)

lideping@hit.edu.cn (Deping Li)

cilijie@hit.edu.cn (Lijie Ci)

**Abstract**

Potassium-ion batteries (PIBs) by virtue of their strong cost competitiveness and similar electrochemical properties to lithium-ion batteries have been deemed to be a promising electrochemical energy storage technology. To promote the application in the commercial market, developing electrode materials with high specific capacities, superior cycling stability, and reliable safety is of great importance. Anode materials as an important component of PIBs play a decisive role, among which two-dimensional transition metal chalcogenides (2D TMCs) have attracted wide attention owing to their unique material and electrochemical properties. In the 2D TMCs' family, molybdenum chalcogenides as flagship are the most studied materials and demonstrated the potential as anodes. With the deepening of research on 2D TMCs, another shining member that possesses similar properties to molybdenum chalcogenides, tungsten chalcogenides ($WS_2$, $WSe_2$, and $WTe_2$), has aroused tremendous attention. Despite many inspiring results, various challenges remain to be further addressed; meanwhile, some results are still unclear and disputed. Herein, this review first introduces their material properties and electrochemical storage mechanisms. Then, we systematically overview the research progress and put forward promoting improvement strategies. Finally, challenges and opportunities that would be future research directions are discussed.

**Keywords:** Electrochemical energy storage, Potassium-ion batteries, Anodes, Tungsten chalcogenides

## 1. Introduction

Environmental and energy crises are gradually becoming serious global issues, and they are tightly bonded because the primary production of energy (*e.g.*, fossil fuel combustion) is currently unable to obtain by pollution-free strategies.[1] To this end, renewable energy that comes from naturally replenishing sources, such as wind power, solar radiation, and geothermal energy, has been developed vigorously with a view to realizing the "green" achievement of energy. However, one obstacle blocking their practical application is that these energy sources are not timely available and unpredictable, and thus they cannot perform their intended roles.[2-3] Fortunately, energy conversion combined with electrochemical energy storage provides a feasible path to efficiently utilize these renewable energy sources. The converted energy is stored in battery systems in electrochemical form and can be used flexibly.[4-10]

Until now, various electrochemical energy storage technologies based on batteries, such as nickel-cadmium, nickel-hydride, lead-acid, and lithium-ion batteries (LIBs), have been successfully developed. In comparison with their counterparts, LIBs exhibit more advanced and reliable properties (*e.g.*, high energy density, long lifespan, and lightweight).[11-17] In this case, LIBs have rapidly dominated the electrochemical energy storage market since the Sony Corporation launched the first commercial product. After thirty years of development, they are now widely used in portable devices and electric vehicles.[18] To meet the rising demand for LIBs, many countries have introduced relevant policies successively to stimulate and promote their further production and development. Nonetheless, the shortage and uneven distribution of global lithium resources in the earth's crust are of great concern, which would potentially lead to uncertainty about the cost and supply.[19-20] In recent years, potassium-ion batteries (PIBs) have aroused increasing attention because of the cost competitiveness

and wide geographic distribution of potassium.[21-28] Besides, there is no alloying reaction between potassium and aluminum, which further reduced the cost of full PIBs. Indeed, the large ionic radius and heavier atomic mass of potassium result in negative effects. However, potassium presents many advantages in certain aspects, such as Stokes radius, melting point, and desolvation energy (Table 1). In addition, PIBs theoretically have a similar energy density to LIBs because the redox potential of $K^+/K$ (−2.93 V *vs.* SHE) is very close to that of $Li^+/Li$ (−3.04 V *vs.* SHE).[29] Herein, it should be emphasized that the development of PIBs is currently for the purpose of complementing LIBs rather than replacing. Therefore, it is foreseeable that these two alkaline ion batteries would cover the electrochemical energy storage market with different cost budgets in the future.[21, 30-31]

It is well known that the performance of PIBs including capacity, lifetime, and rate capability is highly dependent on the electrochemical properties and material characteristics of electrode materials. Therefore, intensive attention has been paid to developing advanced materials as cathodes and anodes.[32] Anodes as an important component that directly determine the safety and long-term cycling life are of critical importance for alkaline ion batteries such a commercialization-oriented research realm.[32-35] Among developed anode materials (*e.g.*, carbonaceous materials, alloying materials, metal compounds, and organic materials), two-dimensional transition metal chalcogenides (2D TMCs) have been considered as a powerful contender.[36-39] 2D TMCs have unique sandwich-like structures characterized by strong in-plane covalent bonds within each layer and weak *van der Waals* forces interaction between neighboring layers.[40-41] Typically, the height between two adjacent layers is 6–7 Å, which allows the intercalation of guest species into the interlayer space.[22] Besides, the large surface-to-volume ratio and the 2D open structure are in favor of the contact and transportation of $K^+$.[42-43] In the family of 2D TMCs, $MoS_2$ is a flagship material due to its ideal 2D structure and has

long research history.[44-46] Recently, tungsten chalcogenides (TCs), including $WS_2$, $WSe_2$, and $WTe_2$, become another popular option because the larger size of tungsten makes the 2D structure regulate easily.[41, 47] In addition, higher industrial consumption of molybdenum and lower amount of molybdenum mineral resources endow the tungsten-based chalcogenides with advantages in future industrial applications.[47] Besides, the lower ion migration barrier of TCs compared with that of molybdenum chalcogenides is conducive to affording better rate capability.[48]

Until now, a few research results have been published on the application of TCs for PIBs; however, there is no review article to systematically introduce and summarize this kind of material. Another key factor that drives us to focus on this topic is the dissimilar and controversial electrochemical ion storage mechanism in different electrochemical systems. According to these considerations, in this review, we systematically summarize the research progress of TCs for PIBs and collect the electrochemical reaction mechanisms and electrochemical information. Besides, some possible improvement strategies are proposed. Finally, current challenges and future opportunities are discussed. We hope that our work shall serve as a reference to further understand the key role of TCs in PIBs and ascertain the existing disputes.

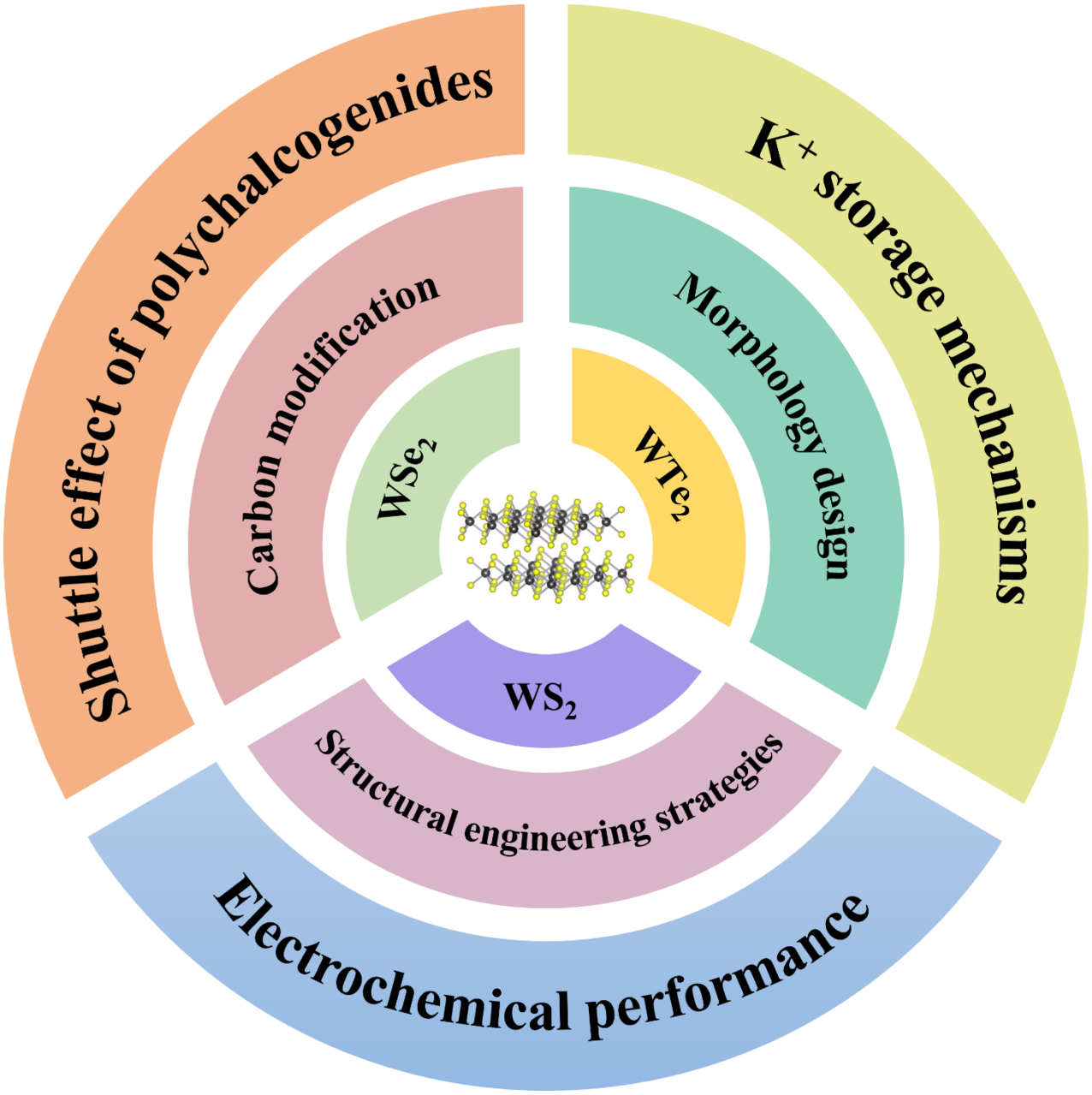


**Fig. 1** Schematic illustration of TCs for PIBs.

**Table 1** Comparison of physical, chemical, and economic properties of Li, Na, and K.

| | **Li** | **Na** | **K** |
|---|---|---|---|
| Atomic number | 3 | 11 | 19 |
| Atomic mass (g $mol^{-1}$) | 6.94 | 22.989 | 39.098 |

| | | | |
|---|---|---|---|
| Ionic radius (Å) | 0.76 | 1.02 | 1.38 |
| Stokes radius in PC (Å) | 4.8 | 4.6 | 3.6 |
| Stokes radius in water (Å) | 2.38 | 1.84 | 1.25 |
| $E^0$ ($A^+_{aq.}$/A) (V *vs*. SHE) | –3.04 | –2.71 | –2.93 |
| $E^0$ ($A^+_{PC}$/A) (V *vs*. $Li^+_{PC}$/Li) | 0 | 0.23 | –0.09 |
| Melting point (°C) | 180.54 | 97.79 | 63.5 |
| Molar conductivity in PC (S $cm^2$ $mol^{-1}$) | 8.3 | 9.1 | 15.2 |
| Desolvation energy in PC (kJ $mol^{-1}$) | 215.8 | 158.2 | 119.2 |
| Abundance in the earth's crust (%) | 0.0017 | 2.36 | 2.09 |
| Distribution | 70% in South America | Everywhere | Everywhere |
| Alloy with aluminum | Yes | No | No |
| Price of carbonate (US $ $ton^{-1}$) | 6500 | 200 | 1000 |
| Price of carbonate (US $ $Mole^{-1}$) | 0.480 | 0.021 | 0.138 |

## 2. Properties of TCs

2D TMCs are famous for their graphite-like layered structures where metals and chalcogens are arranged in a hexagonal structure, resulting in anisotropic electrical, chemical, mechanical, and thermal properties.[40] Owing to different coordination manners between transition metal atoms and

their neighboring chalcogen atoms, 2D TMCs have several structural phases, among which stable semiconducting 1T and metastable metallic 2H phases are two common forms, as illustrated in Fig. 2.[41] In the family of 2D TMCs, TCs possess versatile material properties and thus have been widely applied in electrochemical energy storage, catalysis, optoelectronic devices, solar cells, sensors, spintronics, *etc*. They have a few similar properties to molybdenum counterparts, but their structures are variegated because the large size of tungsten endows them with lattice structural sensitivity, which provides a superior possibility to alter their 2D structures to modulate the material properties.[47] Normally, $WS_2$ and $WSe_2$ are semiconductive, while $WTe_2$ is semimetallic. Their bond length, in-sheet lattice constant, and interlayer spacing increase with increasing the atomic size of chalcogenide elements, as shown in **Table 2**. In theory, 4 mol alkaline ions are able to uptake into TC per formula unit, corresponding to specific capacities of 432 $mAh \cdot g^{-1}$ ($WS_2$), 314 $mAh \cdot g^{-1}$ ($WSe_2$), and 244 $mAh \cdot g^{-1}$ ($WTe_2$). Herein, it is worth emphasizing that the electrochemical reaction of $WS_2$ in PIBs appears to be different from that in LIBs and SIBs based on our research work and some reported results, yielding a much lower specific capacity. However, this mechanism remains controversial with totally different conclusions in reported works.[49-50] The detail will be discussed in later sections.

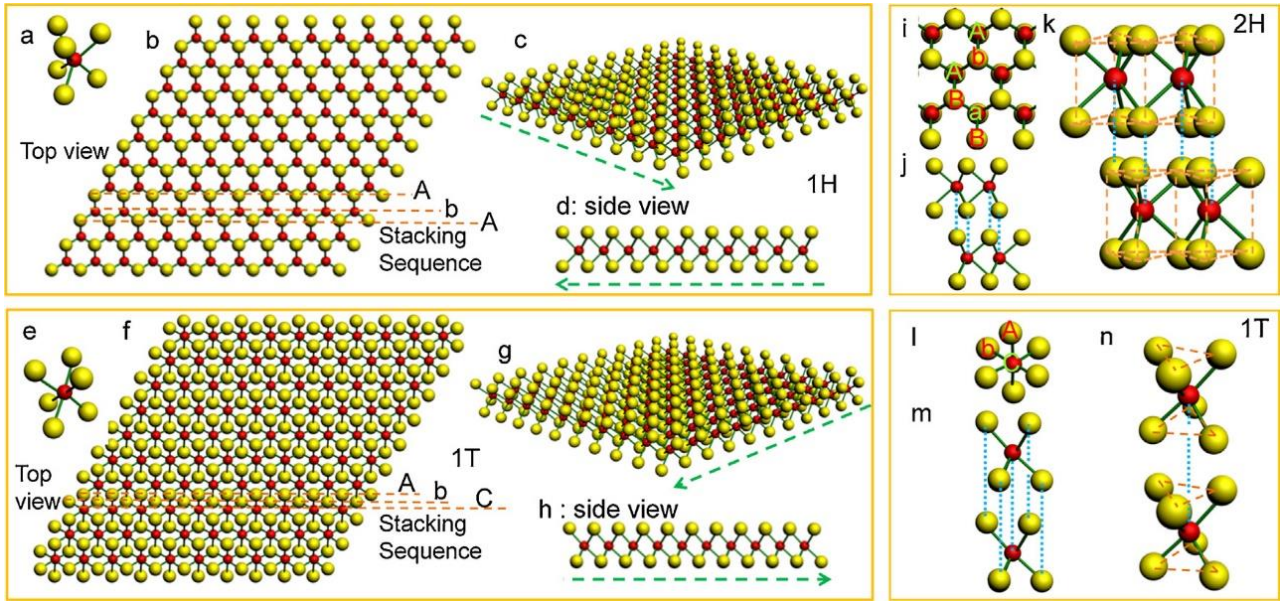


**Fig. 2** (a–h) Schematic crystal structure of single-layer TMCs: (a–d) 1H, hexagonal symmetry, trigonal prismatic coordination, (e–h) 1T, tetragonal symmetry, octahedral coordination. (i–k) Schematics of 2H polytype: two 1H layers per repeat unit, M atoms atop X atoms of the adjacent layer and vice versa, (i) top view, (j–k) side view. (l–n) Schematics of 1T polytype: two 1T layers per repeat unit, M (X) atoms atop M (X) atoms of the adjacent layer, (l) top view, (m and n) side view. Red and yellow balls represent metal and chalcogen atoms, respectively.[41] (Reprinted with permission, Copyright 2020, Wiley).

**Table 2** Properties of $WS_2$, $WSe_2$, and $WTe_2$.[41]

| | **$WS_2$** | **$WSe_2$** | **$WTe_2$** |
|---|---|---|---|
| Molar mass | 247.98 g $mol^{-1}$ | 341.76 g $mol^{-1}$ | 439.04 g $mol^{-1}$ |
| Crystal structure | Hexagonal | Hexagonal | Hexagonal/Orthorhombic |
| Electronic characteristics | Semiconductive | Semiconductive | Semimetallic |

| | | | |
|---|---|---|---|
| Lattice constant | 3.16–3.19 Å | 3.29–3.32 Å | 3.47–3.56 Å |
| Bond length | 2.39–2.42 Å | 2.51–2.55 Å | 2.70–2.74 Å |
| Distance between layers in bulk | 6.08–6.18 Å | 6.41 Å | 6.94–7.03 Å |
| Theoretical specific capacity | 432 mAh·g$^{-1}$ | 314 mAh·g$^{-1}$ | 244 mAh·g$^{-1}$ |

## 3. Applications in PIBs

### 3.1 $WS_2$

$WS_2$ was the first investigated TC-based anode in PIBs. Commercial $WS_2$ powders were directly used to demonstrate the electrochemical $K^+$ storage capability of $WS_2$.[49] $K^+$ intercalation occurred at an average operation potential of 0.72 V *vs*. K/$K^+$ and showed well-defined voltage plateaus, while $Li^+$/$Na^+$ intercalation plateau potential was >1.5 V. Therefore, $WS_2$ as an anode in PIBs offered superiorities over that in LIBs/SIBs when considering the energy density of full cells. During discharging to 0.1 V, 0.62 $K^+$ could insert into per $WS_2$ formula unit, corresponding to a specific capacity of 67 mAh·g$^{-1}$. $WS_2$ transformed to $K_{0.62}WS_2$, accompanied by a small cell volume expansion of 37.81%, which was only one-half that of graphite. After 100 cycles at 5 mAh·g$^{-1}$, the electrode still delivered a reversible capacity of 56.6 mAh·g$^{-1}$ with 84.5% capacity retention. At a high current density of 100 and 150 mA·g$^{-1}$, capacity retentions were as high as 90.8% and 96.3% over 1000 cycles, respectively. Combined with characterization technologies, the high structural stability upon repeated cycling was confirmed (Fig. 3a). When setting a cut-off voltage to 0 V, a higher capacity of 212 mAh·g$^{-1}$ was achieved but the cycling stability significantly deteriorated. As

indicated by the authors, the above phenomenon should be attributed to the reduction of $WS_2$ to W below ~0.08 V (Fig. 3b). In our previous work, we also investigated the electrochemical K storage properties of commercial $WS_2$ powders and found an intercalation-dominated storage mechanism in the full discharge voltage range approaching to 0.01 V.[50] Structural and phase characterizations showed that no metallic W was produced upon $K^+$ intercalation and layered structures was well maintained (Fig. 3c–e). This was quite different from the electrochemical $Li^+$ and $Na^+$ storage mechanisms of $WS_2$ (*i. e.* conversion-type reactions). This unique mechanism might be ascribed to the following factors. First, the $K^+$ diffusion time at the deep discharge condition was too short to ensure the occurrence of conversion processes. Second, the large size of the commercial powders caused kinetic difficulty of the large-radius $K^+$ diffusion. Third, the interlayer spacing was not enough to allow sufficient $K^+$ intercalation, thus the low-concentration $K^+$ could not drive a conversion reaction. In this case, we conducted a series of experiments to rule out these factors, and the results confirmed that the intercalation-dominated $K^+$ storage mechanism was reasonable. Owing to the highly reversible $K^+$ intercalation in the *van der Waals* gaps, the $WS_2$ anode maintained superior cycling stability. Thereafter, another reaction mechanism that comprises the initial intercalation ($WS_2 \rightarrow K_xWS_2$) and subsequent conversion ($K_xWS_2 \rightarrow K_2S_5 \rightarrow W + K_2S$) was proposed.[51] In the initial cyclic voltammetry (CV) profile, there were obvious reduction peaks that might correspond to the conversion reaction from $K_xWS_2$ to $K_2S$ and metallic W. Meanwhile, a high discharge capacity of 543 $mAh \cdot g^{-1}$ was achieved. These observations indicated the occurrence of a conversion reaction. To elucidate the reaction mechanism, *in situ* Raman and *in situ* XRD measurements were conducted (Fig. 3f–g). It was clear that the conversion reaction took place during the initial discharge–charge process.

Above all, three different $K^+$ storage mechanisms of $WS_2$ have been proposed accompanied by convincing theoretical and experimental evidence. However, the reason causing this difference waits for further investigations.

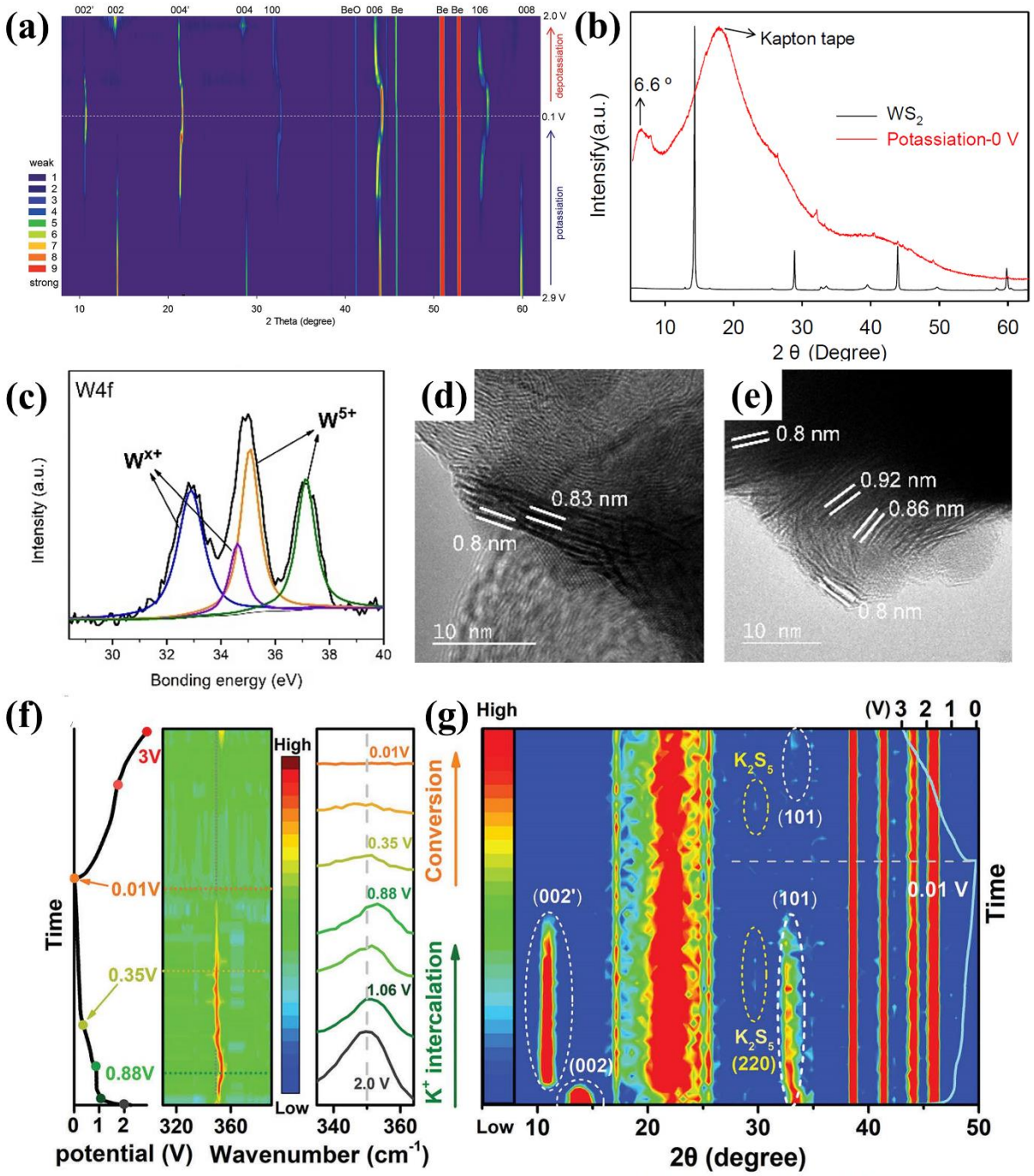


**Fig. 3** (a) *In situ* XRD patterns of commercial $WS_2$ powders collected from the initial cycle. (b) The XRD patterns of initial and potassiated the $WS_2$ anodes at 0 V (*vs.* $K/K^+$). (c) W4f XPS spectrum and

(d–e) HRTEM images of commercial $WS_2$ powders after the first discharge. (f–g) *In situ* Raman mapping and *in situ* XRD patterns of C-$WS_2$@CNFs during the first cycle.[51] (Reprinted with permission, Copyright 2021, The Royal Society of Chemistry).

In later studies, conversion reaction mechanisms held a dominant position, and the main purpose mainly focused on improving the electrochemical performance of $WS_2$ through various strategies. The electrochemical performance of $WS_2$ anodes is mainly limited by severe volume expansion and low electrical conductivity. Combing with carbon materials is an effective method to address these issues. There are two widely adopted ways. The first one is planting $WS_2$ nanosheets on carbon materials. For example, Li *et al*. constructed a freestanding PIB anode of carbon-coated $WS_2$ nanosheets supported on carbon nanofibers (C-$WS_2$@CNFs) (Fig. 4a).[51] The carbon coating inhibited the volume expansion and enhanced the electrical conductivity. As a result, the cycling stability and rate capability were improved obviously (Fig. 4b–c). Zhao and co-workers loaded mixed-phase 1T/2H-$WS_2$ onto nitrogen-doped multichannel carbon nanofibers (1T/2H-$WS_2$/N-MCNFs) to form a flexible current-collector-free PIB anode.[52] Owing to the superior conductivity and multichannel structure, N-MCNFs enabled fast electron and ion transport. The authors studied the effect of mass loading of 1T/2H-$WS_2$ on the electrochemical performance. Three samples with different mass loading (23.8 %, 50.6 %, and 88.3%) all showed good cycling stability, while the sample with 88.3% mass loading had the highest areal capacity. Another one is encapsulating $WS_2$ into carbon materials. For instance, Zeng *et al.* obtained $WS_2$/sulphurized polyacrylonitrile composites ($WS_2$/SPAN) using electrospinning combing with a carbonization process.[53] The composite showed a fibrous 3D network structure that can limit the volume change of $WS_2$ and improve the structural strength of the electrode (Fig. 4d–e). The SPAN fibers contained abundant S vacancies and N doping sites that could absorb

polysulfide generated from electrochemical reactions, thus inhibiting the undesired dissolution and prolonging the cycling life of the electrode material. After 1500 cycles, the reversible capacity maintained 278 $mAh \cdot g^{-1}$ at a current density of 1 $A \cdot g^{-1}$.

Other strategies, such as vacancy chemistry, defect engineering, and heteroatom doping, also exhibit positive effects for $WS_2$ anodes in PIBs. Zhu *et al.* introduced sulfur vacancies into ultrathin $WS_2$ nanosheets ($S_v$-$WS_2$) and investigated the $K^+$ storage capability.[54] The sulfur vacancies (Fig. 4f) enhanced the electrical conductivity and expanded the interlayer spacing, which facilitated electron and ion transport, thereby accelerating the reaction kinetics. In addition, the expanded interlayer spacing could accommodate more $K^+$. Meanwhile, the sulfur vacancies offer more active sites for $K^+$ adsorption. In this case, $S_v$-$WS_2$ delivered higher specific capacities and rate performance in comparison to pristine $WS_2$ nanosheets (without sulfur vacancies) and commercial $WS_2$ powders (Fig. 4g). In the following study, the authors designed selenium doing $S_v$-$WS_2$ nanosheets (Fig. 4h).[55] Density functional theory (DFT) calculations indicated that the introduction of Se not only enhanced the electrical conductivity but also reduced the $K^+$-insertion energy barrier in $WS_2$ nanosheets, resulting in an improved rate capability. Yu and co-workers achieved the fast $K^+$ storage of $WS_2$ by combing N, O co-doping strategies and atomic-interface engineering.[56] During preparation processes, *N*, *N*-dimethylformamide (DMF) was added into precursor solutions, which served as N, O sources and transformed into monolayer carbon between adjacent $WS_2$ layers. With an optimized adding amount of DMF, the cycling performance and reversible capacity are obviously enhanced (Fig. 4i). Besides, its rate capability is still the best among the reported $WS_2$-based PIB anodes, which could be attributed to fast reaction kinetics and strengthened structural stability (Fig. 4j).

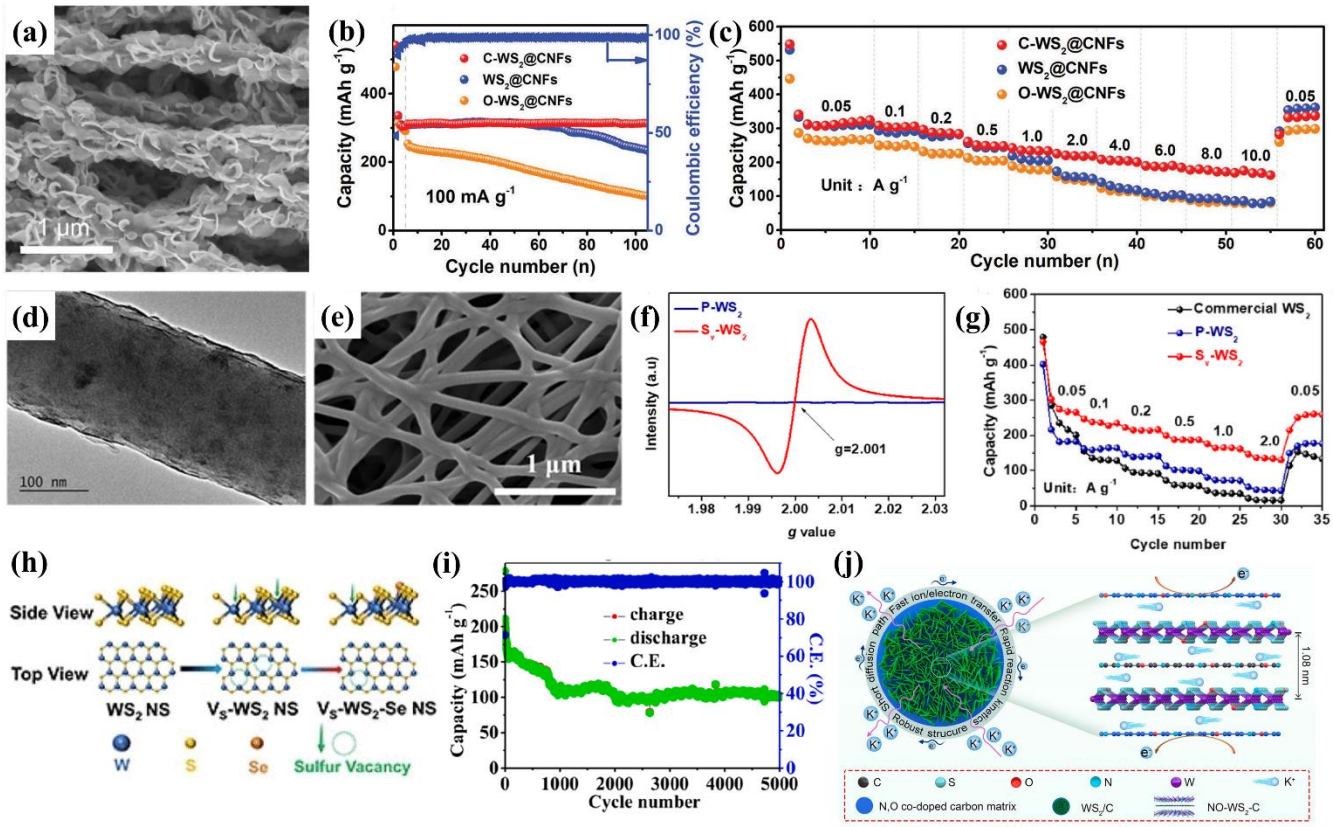


**Fig. 4** (a) SEM image of C-$WS_2$@CNFs. (b–c) Cycling performance at 100 mA·$g^{-1}$ and (d) rate capabilities of C-$WS_2$@CNFs, $WS_2$@CNFs, and O-$WS_2$@CNFs.[51] (Reprinted with permission, Copyright 2021, The Royal Society of Chemistry). (d–e) TEM and SEM images of $WS_2$-SPAN.[53] (Reprinted with permission, Copyright 2023, Elsevier). (f) EPR spectra of $WS_2$ (P-$WS_2$) and $WS_2$ with sulfur vacancies (Sv-$WS_2$). (g) Rate performance of commercial $WS_2$, P-$WS_2$, and $S_v$-$WS_2$.[54] (Reprinted with permission, Copyright 2022, Elsevier). (h) Schematic of $WS_2$ nanosheets ($WS_2$ NS), $WS_2$ with sulfur vacancies ($V_s$-$WS_2$ NS), and selenium filled $V_s$-$WS_2$ nanosheets ($V_s$-$WS_2$-Se NS).[55] (Reprinted with permission, Copyright 2022, American Chemical Society). (i) Cycling performance of $WS_2$/C at 10C. (j) Schematic illustration of the $K^+$ storage mechanism in $WS_2$/C.[56] (Reprinted with permission, Copyright 2022, Elsevier).

### 3.2 $WSe_2$

$WSe_2$ has better electronic conductivity and larger interlayer spacing compared with $WS_2$, which is in favor of electron transfer and interlayer transport of $K^+$. The $K^+$ storage possibility of $WSe_2$ as an anode was first revealed by first-principles calculations.[57] The results indicated that $WSe_2$ was not a good candidate because of its low K adsorption energy. However, subsequent experimental efforts gradually excavated the merits of $WSe_2$ and discarded the dregs.[58-60] In these reports, there is no doubt that $WSe_2$ stores $K^+$ through conversion reactions, as shown in eqn. (1) and (2), as shown in Fig. 5a.[60]

$$WSe_2 + xK^+ + xe^- \rightarrow K_xWSe_2 \quad (1)$$

$$K_xWSe_2 + (4-x)K^+ + (4-x)e^- \rightarrow W + 2K_2Se \quad (2)$$

$WSe_2$ as an electrode material is still limited by unsatisfactory electronic conductivity. Regarding this case, a large number of works paid attention to improving its electronic conductivity by combing carbon materials in a variety of forms. Wang *et al.* synthesized $WSe_2$ nanocrystals embedded in N-doped porous carbon ($WSe_2$/N-PC) through a side-by-side self-assembly method together with the subsequent selenization process.[58] The well-organized nanocrystals could provide abundant active sites for $K^+$ adsorption, while N-PC could not only effectively enhance the conductivity but also alleviate the volume variation. Qian and co-workers utilized chlorella containing large amounts of nitrogen and phosphorus as a precursor to construct ultrathin few-layered $WSe_2$ anchored on N, P dual-doped carbon (Fig. 5b).[59] Ultrathin $WSe_2$ nanosheets provided more $K^+$ storage sites and shortened the transport length of $K^+$ and electrons. Defect-rich N, P doped biochar ensured the structural stability and high conductivity of the electrode. Serving as a PIB anode, the composite exhibited impressive long-term cycling life (155 $mAh \cdot g^{-1}$ at 1.0 $A \cdot g^{-1}$ after 5300 cycles), as shown in Fig. 5c. Besides, carbon coating is a more promising way to inhibit the volume expansion of $WSe_2$. To this end, a core-shell $WSe_2$@N-doped carbon nanotube was designed (Fig. 5d) and delivered good

cycling stability at both low and high current densities.[61] In 2D TMCs, there exists a special carbon modification, that is *in situ* forming carbon layers between the neighboring layers. For example, Wang *et al.* used oleylamine (OLA) as an adjuvant agent to prepare $WSe_2$/C nanoflowers.[60] During the reaction process, OLA molecules were trapped in the interlayer of $WSe_2$ and converted into amorphous carbon after being annealed at a high temperature of 550 ℃. The carbon expanded the interlayer spacing from 0.651 to 0.755 nm, providing more active sites and fast $K^+$ diffusion channels, as well as enough room to accommodate the volume change of $WSe_2$. In addition, partial OLA molecules coated onto the surface of $WSe_2$ nanoflowers and also transformed into a carbon coating layer during the annealing process, which buffers the volume expansion of $WSe_2$ nanosheets. When it was employed as a PIB anode, the specific capacity retained 384 $mAh \cdot g^{-1}$ at 0.1 $A \cdot g^{-1}$ after 200 cycles, and the capacity retention was as high as 99%.

Cation pre-intercalation has been widely recognized as an effective strategy in improving the electrochemical performance of electrode materials, which was also adopted to modulate $WSe_2$ anodes for PIBs. $K^+$ pre-intercalated single-phased $WSe_2$ nanorod bundles (SP-$K_xWSe_2$) were prepared *via* a hydrothermal pre-potassiation method (Fig. 5e).[62] The sample of $WSe_2$ without $K^+$ pre-intercalation (SP-$WSe_2$) delivered a high capacity of ~400 $mAh \cdot g^{-1}$ in the initial stage, but the capacity rapidly decayed to 180 and 95 $mAh \cdot g^{-1}$ after 20 and 100 cycles, respectively. The poor cycling stability might be attributed to the irreversible lattice fracture causing active material dissolution. SP-$K_xWSe_2$ had the same phase as SP-$WSe_2$, except for a low-angle shifted (002) peak, indicating an expanded interlayer spacing. The schematic is illustrated in Fig. 5f. Additionally, the presence of $K^+$ in the interlayer could improve both the $K^+$ diffusion kinetics and structural stability. Therefore, the SP-$K_xWSe_2$ electrode exhibited excellent cyclability with 89.3% capacity retention

after 5000 cycles (Fig. 5g). The introduction of $K^+$ effectively prevented the loss of W and Se species towards electrolytes and meanwhile, improved the electronic and ionic conductivity, which resulted in the enhanced cycling stability and superior rate capability.

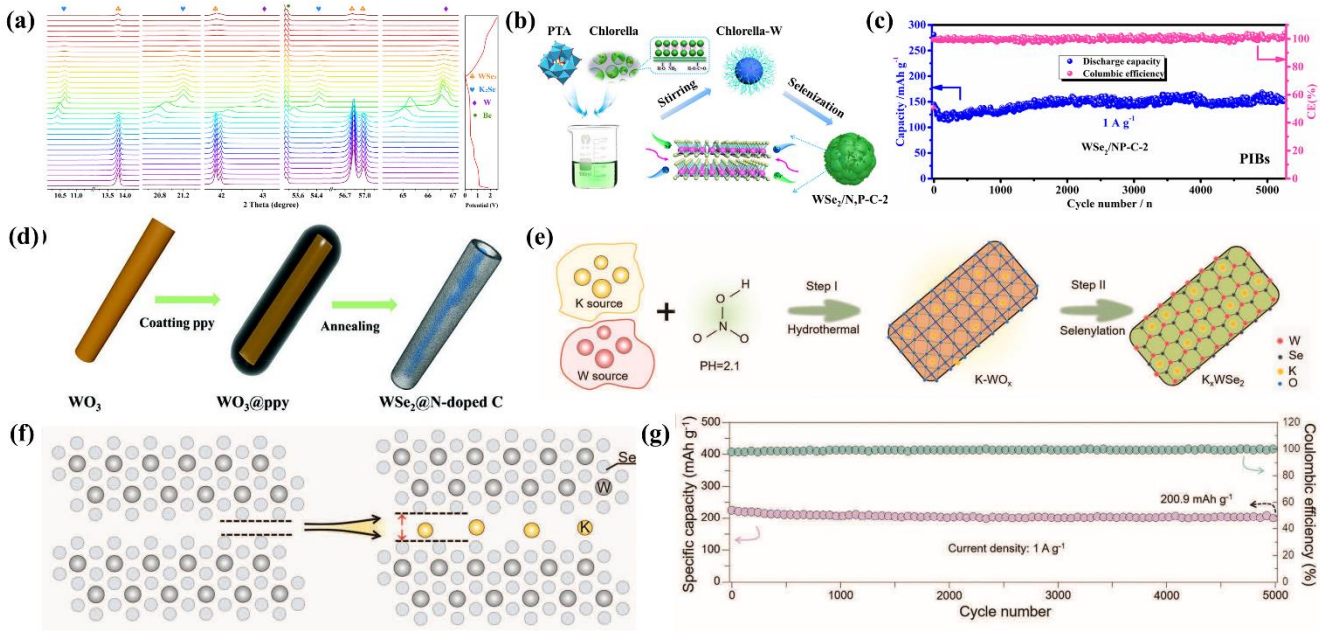


**Fig. 5** (a) *In situ* XRD patterns and the corresponding discharge–charge profiles of c-$WSe_2$.[60] (Reprinted with permission, Copyright 2021, Elsevier). (b) Schematic illustration of the preparation of $WSe_2$/N, P-C composite. (c) Long-term cycling performance at 1.0 $A{\cdot}g^{-1}$ and Coulombic efficiency of $WSe_2$/N, P-C-2.[59] (Reprinted with permission, Copyright 2020, Elsevier). (d) Schematic illustration of the synthesis of $WSe_2$@N-doped C nanorods.[61] (Reprinted with permission, Copyright 2020, Wiley). (e) Schematic illustration of the synthesis of $K_xWSe_2$. (f) Structural evolutions of $WSe_2$ during the "hydrothermal potassiation" process. (g) Long-term cycle performance of SP-$K_xWSe_2$ at 1.0 $A{\cdot}g^{-1}$.[62] (Reprinted with permission, Copyright 2023, Wiley).

### 3.3 $WTe_2$

$WTe_2$ is a semimetallic material and thus shows good conductivity (Fig. 6a),[40] which has also been employed as the anode material for PIBs. Singh's group conducted the earliest studies on the $K^+$

storage behavior and capability of $WTe_2$ using commercial $WTe_2$ as a demonstrator.[63-64] According to a discharging profile, they deduced that per $WTe_2$ molecule could store up to 3.3 $K^+$. Compared with commercial $WS_2$, $WTe_2$ delivered better electrochemical performance in both rate capability and cycling performance (Fig. 6b–c), which might be due to conversion-type reaction-controlled $K^+$ storage (eqn. (3) and (4)) (Fig. 6d). Nonetheless, its cycling stability was unsatisfactory, and the capacity decayed obviously within only dozens of cycles. Anyway, the research on $WTe_2$-based PIB anodes is still in its infant stage, the battery performance will be gradually improved by the joint efforts of researchers.

$$WTe_2 + xK^+ + xe^- \rightarrow K_xWTe_2 \quad (3)$$

$$K_xWTe_2 + xK^+ + xe^- \rightarrow W + 2K_xTe \quad (4)$$

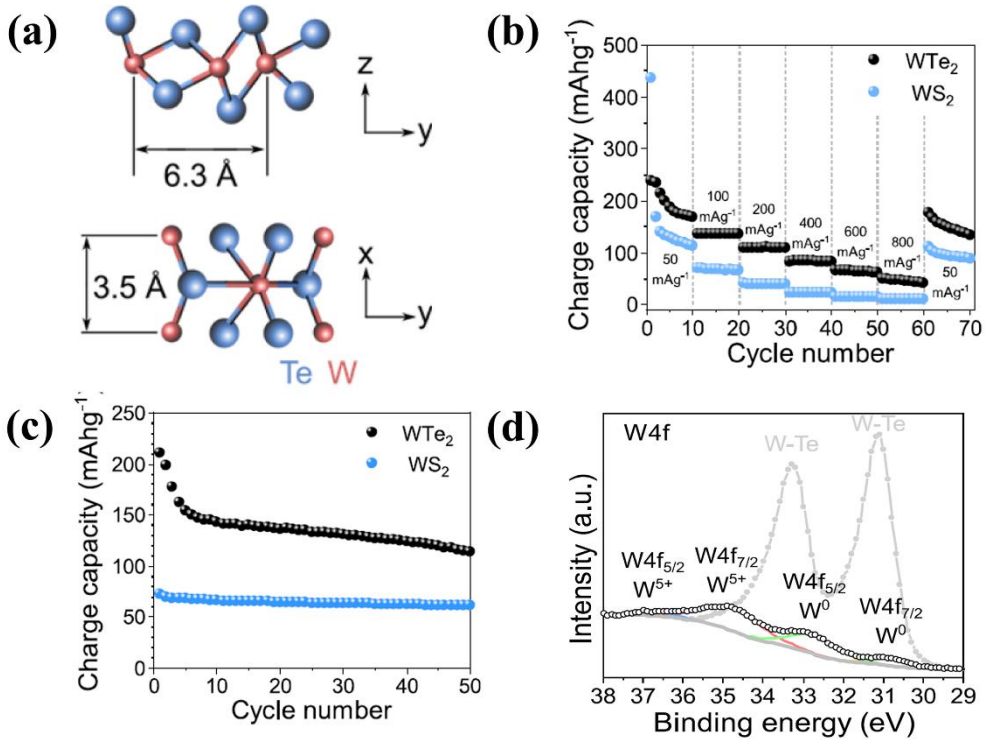


**Fig. 6** (a) Schematic Td-$WTe_2$ phase structure. (b) Rate capability and (c) cycling performance (0.1 $A \cdot g^{-1}$) of $WS_2$ and $WTe_2$. (d) W4f XPS spectrum of $WTe_2$ after discharge.[63] (Reprinted with permission, Copyright 2020, IOP publishing).

## 4. Possible improvement strategies of TCs

TCs, as typical members of TMCs, exhibit many similar merits and issues with other members, such as volume expansion, low conductivity, and the "shuttle effect". In this case, the strategies that are used by other members may be applicable to TCs. This section will introduce some possible strategies for enhancing material properties and improving electrochemical performance, including carbon modification, morphology design, and structural engineering strategies.

### 4.1 Carbon modification

Carbon modification is namely a way to combine TCs with carbon materials (*e.g.,* graphene, carbon nanotubes, and biochar) to form composites, which can address many problems faced by TC anodes. As mentioned above, TC-based anode materials suffer sluggish reaction kinetics. This issue can be offset by introducing carbon materials because they can provide good electron transfer pathways.[38] In addition, carbon materials play two important roles. First, TCs face the problem of severe volume variation during potassiation–depotassiation processes, which may lead to electrode pulverization. When carbon materials are coated onto TCs, the confinement effect provided by carbon materials can buffer the volume change.[65-66] Second, polychalcogenides produced from conversion reactions have high solubility in electrolytes, leading to the "shuttle effect" that is considered to be a key reason for the poor cyclability, inferior reversibility, and low round-trip efficiencies efficiency of TCs.[21, 67-69] Carbon materials with high adsorption or polar functional groups can effectively grasp the polychalcogenides and suppress the "shuttle effect".[70-71]

### 4.2 Morphology design

The morphology of electrode materials acts as a critical role in electrochemical reaction kinetics and electrochemical performance. Downsizing electrode materials to the nanoscale can make TCs exhibit

superior material properties, thereby enhancing electrochemical performance.[72-73] Nanosized TCs can expose abundant active sites for $K^+$ adsorption. In the meantime, the ion and electron diffusion lengths in TCs are dramatically shortened, which promotes the electrochemical reaction kinetics. Designing TCs with special morphologies, such as ordered mesoporous,[74] nanowires,[75] and nanoflowers,[76] is also a promising way. Apart from the above-mentioned advantage, well-designed TCs normally exhibit structural stability during electrochemical cycling because unique morphological structures can provide room to accommodate volume expansion.

**4.3 Structural engineering strategies**

Structural engineering strategies, such as heteroatom doping, defect chemistry, interlayer expansion, and crystallinity regulation, are widely used in materials science, which can modulate material intrinsic properties and endow materials with novel properties. Heteroatom doping and defect chemistry can regulate the electronic structure and physicochemical properties of TMCs, reduce charge transfer resistance, generate new active sites, and expand the interlayer spacing of TMCs, which significantly improves ion storage capability and reaction kinetics.[77-80] All TCs have layered structures, and their interlayer spacing provides natural room and pathways for ion storage and diffusion. Therefore, expanding the interlayer spacing is promising to achieve electrochemical performance enhancement. When the interlayer expansion is realized by inserting carbon materials/conductive polymers, the electronic conductivity and structural stability of TCs can be enhanced.[81] The crystallinity of 2D TMCs determines the electrochemical $K^+$ storage behavior and performance controlled by different reaction mechanisms.[82] In this case, TCs for different energy storage applications can be obtained by regulating the crystallinity.

## 5. Conclusions and outlook

PIBs as an emerging electrochemical storage technology have aroused prominent attention in the past few years. They own many advantages and display great potential as promising supplements to LIBs. Nonetheless, there are numerous problems and challenges in this new field. One is the lack of high-performance anode materials. TCs that are widely investigated in various battery systems deliver good $K^+$ storage capability (Table 3). Until now, the reported works on TC anodes are relatively limited, especially $WTe_2$. The low abundance and high price of Te may be a possible reason. TC-based anode materials are largely struggling with severe volume changes, unsatisfactory electronic conductivity, sluggish reaction kinetics, and the "shuttle effect". In Section 4, we provide some possible ways that may solve or alleviate these problems. Besides, the strategies adopted by other TMCs are possible to be applied.

In this review, we systematically introduce the recent research advance in TCs for PIB anodes. The electrochemical information including electrolytes, electrochemical performance, and voltage windows are collected in Table 3. According to the experiences and knowledge obtained from other TMC anodes, some possible improvement strategies toward the material properties and electrochemical performance are put forward. By summarizing the research progress, we believe that some further and deep studies are necessary.

**(1) Unveiling $K^+$ storage mechanisms.** $WS_2$ is the most studied TC, and its $K^+$ storage mechanism was investigated by several works. However, as mentioned above, the obtained mechanisms were quite different, including conversion at low voltages, intercalation, and conversion types. The authors all gave sufficient evidence to verify the reasonableness of their obtained results. It is necessary to consider what factors result in such a big difference. From our point of view, this

may originate from material intrinsic properties or test/characterization methods. Therefore, future studies should pay more attention to this case. As for $WSe_2$, its $K^+$ storage mechanism is uncontroversial. *i.e.*, conversion types. So far, the reports on $WTe_2$ are extremely limited, and there is not adequate evidence to reveal the $K^+$ storage mechanism. The investigation on its mechanism is also important in future research directions.

**(2) Improving electrochemical performance.** Although encouraging research results were achieved, most obtained electrochemical performance and reaction kinetics was unsatisfactory. There is still much improvement room. Three promising strategies (*i.e.*, carbon modification, morphology structure design, and engineering strategies) toward material design put forward in Section 4 may be effective options. They mainly enhance the electrochemical performance by strengthening material structures, exposing active sites, and accelerating ion and electron transfer. Besides, electrolytes play critical roles in determining the electrochemical performance. Suitable solvents can relieve the "shuttle effect" of polychalcogenides, optimize solid-electrolyte interphase (SEI) layers, and inhibit K dendrites, which have great effects on battery lifespan and safety.[83-85] Salts in electrolytes should also be considered because different salts show different properties, such as ionic conductivity and electrochemical stability.[86] Here, it should be emphasized that the cost of salts cannot be ignored in pursuit of electrochemical performance.

**(3) Inhibiting the dissolution and side reactions of polychalcogenides in electrolytes**. During electrochemical reaction processes, TMCs produce polychalcogenides that may lead to poor cycling stability and unsatisfactory round-trip efficiency.[67] In PIBs, there are two commonly used electrolytes, carbonate ester-based and ether-based electrolytes. The carbonate ester-based electrolytes show better electrochemical stability at high voltage ranges. However, they may be exhausted during

electrochemical reactions because they can react with polychalcogenides to generate thiocarbonates. Ether-based electrolytes possess the advantages of optimizing the composition of SEI, promoting charge transfer, and reinforcing the geometric architecture of electrode materials.[83, 87] Nevertheless, their high solubility against polychalcogenides leads to the "shuttle effect". We believe that this problem also exists in TC-based PIB anodes. Unfortunately, this was scarcely considered in the reported works. Future research can draw on advanced experience and skills gained from Li/Na/K-S/Se batteries.[88-90]

All in all, although the potential and capabilities of TCs as PIB anodes have been preliminarily explored, there still are many unclear and unsolved issues. We hope this review shall provide valuable information and suggestions to facilitate the further development of TCs.

**Table 3** Electrochemical information of reported TC-based PIB anodes.

| Materials | Voltage ranges | Electrolytes | Cycling stability | Rate capability |
|---|---|---|---|---|
| | | **$WS_2$** | | |
| Commercial $WS_2$ powders[49] | 0.1–2.0 V | 5.0 M KFSI in DEGDME | 56.6 $mAh \cdot g^{-1}$ at 0.005 $A \cdot g^{-1}$ after 100 cycles<br>40 $mAh \cdot g^{-1}$ at 0.2 $A \cdot g^{-1}$ after 500 cycles | |
| Commercial $WS_2$ powders[50] | 0.01–3.0 V | 1.0 M $KPF_6$ in PC/EC (1:1) | 103 $mAh \cdot g^{-1}$ at 0.1$A \cdot g^{-1}$ after 100 cycles | |
| $WS_2$/graphene[91] | 0.1–1.5 V | 5.0 M KFSI in DEGDME | 74 $mAh \cdot g^{-1}$ at 0.02 $A \cdot g^{-1}$ after 50 cycles<br>36 $mAh \cdot g^{-1}$ at 0.05 $A \cdot g^{-1}$ after 500 cycles | 32 $mAh \cdot g^{-1}$ at 200 $mA \cdot g^{-1}$ |
| C-$WS_2$@CNFs[51] | 0.01–3.0 V | 1.0 M KFSI in EC/DMC (1:1) | 321 $mAh \cdot g^{-1}$ at 0.1 $A \cdot g^{-1}$ after 100 cycles<br>168 $mAh \cdot g^{-1}$ at 2.0 $A \cdot g^{-1}$ after 300 cycles | |

| | | | |
|---|---|---|---|
| $WS_2$ nano-plates[92] | 0.01–2.0 V | 0.8 M $KPF_6$ in EC/DEC | 250 $mAh·g^{-1}$ at 0.1 $A·g^{-1}$ after 50 cycles |
| $WS_2$ nanosheets with S vacancies[54] | 0.01–3.0 V | 1.0 M KFSI in PC/EC (1:1) | 230.8 $mAh·g^{-1}$ at 0.1 $A·g^{-1}$ after 50 cycles |
| Se-filled $WS_2$ nanosheets with S vacancies[55] | 0.01–3.0 V | 1.0 M KFSI in PC/EC (1:1) | 328.6 $mAh·g^{-1}$ at 0.1 $A·g^{-1}$ after 50 cycles<br>144.2 $mAh·g^{-1}$ at 2.0 $A·g^{-1}$ after 100 cycles |
| N, O co-doping $WS_2$/C[56] | 0.01–3.0 V | 1.0 M KFSI in EC/DEC (1:1) | 422.8 $mAh·g^{-1}$ at 0.1C after 100 cycles<br>163.8 $mAh·g^{-1}$ at 5C after 5000 cycles |
| 1T/2H-$WS_2$ nanosheets on N-doped multichannel CNFs[52] | 0.01–2.6 V | | 2.63 $mAh·cm^{-2}$ at 1.4 $mA·cm^{-2}$ after 200 cycles<br>1.21$mAh·cm^{-2}$ at 14 $mA·cm^{-2}$ after 1000 cycles |
| $WS_2$–SPAN nanofibers[53] | 0.01–3.0 V | 1.0 M KFSI in DME | 362 $mAh·g^{-1}$ at 0.1 $A·g^{-1}$ after 100 cycles<br>278 $mAh·g^{-1}$ at 1.0 $A·g^{-1}$ 3000 cycles |

| $WSe_2$ | | | | |
|---|---|---|---|---|
| $WSe_2$/N-doped porous carbon[58] | 0.005–3.0 V | 0.8 M $KPF_6$ in EC/DEC (1:1) | 390 mAh·$g^{-1}$ at 0.1 A·$g^{-1}$ after 200 cycles<br>316 mAh·$g^{-1}$ at 0.2 A·$g^{-1}$ after 200 cycles<br>184 mAh·$g^{-1}$ at 0.8 A·$g^{-1}$ after 400 cycles | 184 mAh·$g^{-1}$ at 1.6 A·$g^{-1}$ |
| $WSe_2$/N, P dual-doped carbon[59] | 0.01–3.0 V | 3.0 M KFSI in DME | 333 mAh·$g^{-1}$ at 0.1 A·$g^{-1}$ after 100 cycles<br>155 mAh·$g^{-1}$ at 1 A·$g^{-1}$ after 5300 cycles | |
| $WSe_2$/C[60] | 0.01–2.5 V | 3.0 M KFSI in DME | 384 mAh·$g^{-1}$ at 0.1 A·$g^{-1}$ after 200 cycles<br>209 mAh·$g^{-1}$ at 1.0 A·$g^{-1}$ after 500 cycles | |
| Commercial $WSe_2$ powders[93] | 0.1–2.0 V | 3.0 M KFSI in DEGDME | 144.4 mAh·$g^{-1}$ at 0.005 A·$g^{-1}$ after 50 cycles<br>112 mAh·$g^{-1}$ at 0.1 A·$g^{-1}$ after 100 cycles | |

| | | | | |
|---|---|---|---|---|
| $WSe_2$/CNTs[61] | 0.01–2.6 V | 3.0 M KFSI in DEGDME | 301.7 mAh·$g^{-1}$ at 0.1 A·$g^{-1}$ after 120 cycles<br>122.1 mAh·$g^{-1}$ at 0.5 A·$g^{-1}$ after 1300 cycles | |
| $K^+$-single-phased $WSe_2$[62] | 0.01–3.0 V | 1.0 M $KPF_6$ in EC/DEC (1:1) | 401.2 mAh·$g^{-1}$ at 0.1 A·$g^{-1}$ after 1000 cycles<br>200.9 mAh·$g^{-1}$ at 1.0 A·$g^{-1}$ after 5000 cycles | 211 mAh·$g^{-1}$ at 5.0 A $g^{-1}$ |
| Sn-doped 1T-$WSe_2$[94] | 0.01–3.0 V | 3.0 M KFSI in DME | 345 mAh·$g^{-1}$ at 0.1 A·$g^{-1}$ after 50 cycles<br>120 mAh·$g^{-1}$ at 1.0 A·$g^{-1}$ after 1000 cycles | |
| $WSe_2$/P, N dual-doped carbon[95] | 0.01–3.0 V | 1.0 M KFSI in EMC | 277.7 mAh·$g^{-1}$ at 0.1 A·$g^{-1}$ after 100 cycles<br>112.2 mAh·$g^{-1}$ at 2.0 A·$g^{-1}$ after 2500 cycles | 95 mAh·$g^{-1}$ at 5.0 A·$g^{-1}$ |
| **$WTe_2$** | | | | |

| | | | | |
|---|---|---|---|---|
| Commercial $WTe_2$ powders[63] | 0.01–3.0 V | 1.0 M $KPF_6$ in EC/DEC (1:1) | 136.2 $mAh \cdot g^{-1}$ at 0.1 $A \cdot g^{-1}$ after 150 cycles | 50.12 $mAh \cdot g^{-1}$ at 0.8 $A \cdot g^{-1}$ |
| Td-$WTe_2$[64] | 0.01–3.0 V | 1.0 M $KPF_6$ in PC/EC (1:1) | 172 $mAh \cdot g^{-1}$ at 0.05 $A \cdot g^{-1}$ 60 cycles | |

## Appendix

| Abbreviations | Full name |
|---|---|
| EC | Ethylene carbonate |
| PC | Propylene carbonate |
| DEC | Diethyl carbonate |
| EMC | Ethyl methyl carbonate |
| DME | Dimethoxyethane |
| DMC | Dimethyl carbonate |
| DEGDME | Diethylene glycol dimethyl ether |
| $KPF_6$ | Potassium hexafluorophosphate |
| KFSI | Potassium bis(fluorosulfonyl)imide |


## Acknowledgments

This work was supported by the National Natural Science Foundation of China (Grant No. 52002094), the Shenzhen Steady Support Plan (GXWD20221030205923001), the Guangdong Basic and Applied Basic Research Foundation (Grant No. 2019A1515110756), the Shenzhen Science and Technology Program (Grant No. JCYJ20210324121411031, JSGG202108021253804014, RCBS20210706092218040), the Open Fund of the Guangdong Provincial Key Laboratory of Advanced Energy Storage materials (Grant. No. asem202107), and the Shenyang University of Technology (QNPY202209-4).


## Declare of Interests

The authors declare no conflict of interest.

**References**


1. Balat M. Usage of energy sources and environmental problems. Energ Explor Exploit. 2005; 23:141.

2. Goodenough JB, Park KS. The Li-ion rechargeable battery: a perspective. J Am Chem Soc. 2013; 135:1167.

3. Xu Y, Zhou M, Lei Y. Nanoarchitectured Array Electrodes for Rechargeable Lithium- and Sodium-Ion Batteries. Adv Mater. 2016;6:1502514.

4. Jeong G, Kim Y-U, Kim H, Kim Y-J, Sohn H-J. Prospective materials and applications for Li secondary batteries. Energy Environ. Sci. 2011;4:1986.

5. Kundu D, Talaie E, Duffort V, Nazar LF. The emerging chemistry of sodium ion batteries for electrochemical energy storage. Angew Chem Int Ed. 2015;54:3431.

6. Wu Y, Wu X, Guan Y, Xu Y, Shi F, Liang J. Carbon-based flexible electrodes for electrochemical potassium storage devices. New Carbon Mater. 2022;37:852.

7. Wu Y, Chen G, Wu X, Li L, Yue J, Guan Y, Hou J, Shi F, Liang J. Research progress on vanadium oxides for potassium-ion batteries. J Semicond. 2022;43:1.

8. Wang H, Yang Q, Zheng N, Zhai X, Xu T, Sun Z, Wu L, Zhou M. Roadmap of amorphous metal-organic framework for electrochemical energy conversion and storage. Nano Res. 2022;16:4107

9. Xue H, Gong H, Yamauchi Y, Sasaki T, Ma R. Photo-enhanced rechargeable high-energy-density metal batteries for solar energy conversion and storage. Nano Res Energy. 2022;1:9120007.

10. Lv J, Wang B, Hao J, Ding H, Fan L, Tao R, Yang H, Zhou J, Lu B. Single-crystalline Mn-based oxide as a high-rate and long-life cathode material for potassium-ion battery. eScience. 2023;3:100081.

11. Dunn B, Kamath H, Tarascon J-M. Electrical energy storage for the grid: a battery of choices. Science. 2011;334:928.

12. Reddy MV, Subba Rao GV, Chowdari BV. Metal oxides and oxysalts as anode materials for Li ion batteries. Chem Rev. 2013;113:5364.

13. Chen L, Wu H, Ai X, Cao Y, Chen Z. Toward wide-temperature electrolyte for lithium–ion batteries. Battery Energy. 2022;1:20210006.

14. Zhou Y, Zhang Z, Zhang H, Li Y, Weng Y. Progress and perspective of vanadium-based cathode materials for lithium ion batteries. Tungsten. 2021;3:279.

15. Zeng J, Yang L, Shao R, Zhou L, Utetiwabo W, Wang S, Chen R, Yang W. Mesoscopic $Ti_2Nb_{10}O_{29}$ cages comprised of nanorod units as high-rate lithium-ion battery anode. J Colloid Interface Sci. 2021;600:111.

16. Yang L, Zeng J, Zhou L, Shao R, Utetiwabo W, Tufail MK, Wang S, Yang W, Zhang J. Orderly defective superstructure for enhanced pseudocapacitive storage in titanium niobium oxide. Nano Res. 2021;15:1570.

17. Zhou X, Wan LJ, Guo YG. Binding $SnO_2$ nanocrystals in nitrogen-doped graphene sheets as anode materials for lithium-ion batteries. Adv Mater. 2013;25:2152.

18. Nitta N, Wu F, Lee JT, Yushin G. Li-ion battery materials: present and future. Mater Today. 2015;18:252.

19. Kubota K, Dahbi M, Hosaka T, Kumakura S, Komaba S. Towards K-Ion and Na-Ion Batteries as "Beyond Li-Ion". Chem Rec. 2018;18:459.

20. Xu J, Xu Y, Lai C, Xia T, Zhang B, Zhou X. Challenges and perspectives of covalent organic frameworks for advanced alkali-metal ion batteries. Sci China Chem. 2021;64:1267.

21. Wu Y, Zhang C, Zhao H, Lei Y. Recent advances in ferromagnetic metal sulfides and selenides as anodes for sodium- and potassium-ion batteries. J Mater Chem A. 2021;9:9506.

22. Tan H, Feng Y, Rui X, Yu Y, Huang S. Metal Chalcogenides: Paving the Way for High-Performance Sodium/Potassium-Ion Batteries. Small Methods. 2019;4:1900563.

23. Yabuuchi N, Kubota K, Dahbi M, Komaba S. Research development on sodium-ion batteries. Chem Rev. 2014;114:11636.

24. Hosaka T, Kubota K, Hameed AS, Komaba S. Research Development on K-Ion Batteries. Chem Rev. 2020;120:6358.

25. Li D, Ji F, Liu T, Zhao X, Sun Q, Liu Y, Wang Y, Zhang J, Ci L. Trash to treasure: recycling discarded agarose gel for practical Na/K-ion batteries. J Mater Chem A. 2022;10:15026.

26. Feng Y, Lv Y, Fu H, Parekh M, Rao AM, Wang H, Tai X, Yi X, Lin Y, Zhou J, Lu B. Co-activation for enhanced K-ion storage in battery anodes. Natl Sci Rev. 2023;nwad118.

27. Shen M, Ding H, Fan L, Rao AM, Zhou J, Lu B. Neuromorphic Carbon for Fast and Durable Potassium Storage. Adv Funct Mater. 2023;33:2213362.

28. Peng J, Yi X, Fan L, Zhou J, Lu B. Molecular extension engineering constructing long-chain organic elastomeric interphase towards stable potassium storage. Energy Lab. 2023;1:220014.

29. Du Y, Yi Z, Chen B, Xu J, Zhang Z, Bao J, Zhou X. $Sn_4P_3$ nanoparticles confined in multilayer graphene sheets as a high-performance anode material for potassium-ion batteries. J Energy Chem. 2022;66:413.

30. Xiong J, Yang Z, Guo X, Wang X, Geng C, Sun Z, Xiao A, Zhuang Q, Chen Y, Ju Z. Review on recent advances of inorganic electrode materials for potassium-ion batteries. Tungsten. 2022. https://doi.org/10.1007/s42864-022-00177-y

31. Wang X, Wang H. Designing carbon anodes for advanced potassium-ion batteries: Materials, modifications, and mechanisms. Adv Powder Mater. 2022;1:100057.

32. Wu X, Leonard DP, Ji X. Emerging Non-Aqueous Potassium-Ion Batteries: Challenges and Opportunities. Chem Mater. 2017;29:5031.

33. Li L, Zheng Y, Zhang S, Yang J, Shao Z, Guo Z. Recent progress on sodium ion batteries: potential high-performance anodes. Energy Environ Sci. 2018;11:2310.

34. Lu J, Chen Z, Pan F, Cui Y, Amine K. High-Performance Anode Materials for Rechargeable Lithium-Ion Batteries. Electrochem Energy Rev. 2018;1:35.

35. Wu Y, Xu R, Wang Z, Hao X, Zhang C, Zhao H, Li W, Wang S, Dong Y, Huang Z, Lei Y. Carbon-Free Crystal-like $Fe_{1-x}S$ as an Anode for Potassium-Ion Batteries. ACS Appl Mater Interfaces. 2021;13:55218.

36. Zhang Y, Zhang L, Lv T, Chu PK, Huo K. Two-Dimensional Transition Metal Chalcogenides for Alkali Metal Ions Storage. ChemSusChem. 2020;13:1114.

37. Li D, Dai L, Ren X, Ji F, Sun Q, Zhang Y, Ci L. Foldable potassium-ion batteries enabled by free-standing and flexible $SnS_2$@C nanofibers. Energy & Environmental Sci. 2021;14:424.

38. Wu Y, Zhang Q, Xu Y, Xu R, Li L, Li Y, Zhang C, Zhao H, Wang S, Kaiser U, Lei Y. Enhanced Potassium Storage Capability of Two-Dimensional Transition-Metal Chalcogenides Enabled by a Collective Strategy. ACS Appl Mater Interfaces. 2021;13:18838.

39. Du Y, Zhang Z, Xu Y, Bao J, Zhou X. Metal Sulfide-Based Potassium-Ion Battery Anodes: Storage Mechanisms and Synthesis Strategies. Acta Phy Chim Sin. 2022;38:2205017.

40. Chhowalla M, Shin HS, Eda G, Li LJ, Loh KP, Zhang H. The chemistry of two-dimensional layered transition metal dichalcogenide nanosheets. Nat Chem. 2013;5:263.

41. Mohl M, Rautio AR, Asres GA, Wasala M, Patil PD, Talapatra S, Kordas K. 2D Tungsten Chalcogenides: Synthesis, Properties and Applications. Adv Mater Interfaces. 2020;7:2000002.

42. Huang J, Wei Z, Liao J, Ni W, Wang C, Ma J. Molybdenum and tungsten chalcogenides for lithium/sodium-ion batteries: Beyond $MoS_2$. J Energy Chem. 2019;33:100.

43. Wu Y, Yu Y. 2D material as anode for sodium ion batteries: Recent progress and perspectives. Energy Storage Mater. 2019;16:323.

44. Xu Y, Bahmani F, Zhou M, Li Y, Zhang C, Liang F, Kazemi SH, Kaiser U, Meng G, Lei Y. Enhancing potassium-ion battery performance by defect and interlayer engineering. Nanoscale Horiz. 2019;4:202.

45. Dong Y, Xu Y, Li W, Fu Q, Wu M, Manske E, Kroger J, Lei Y. Insights into the Crystallinity of Layer-Structured Transition Metal Dichalcogenides on Potassium Ion Battery Performance: A Case Study of Molybdenum Disulfide. Small. 2019;15:1900497.

46. Dong H, Xu Y, Zhang C, Wu Y, Zhou M, Liu L, Dong Y, Fu Q, Wu M, Lei Y. $MoS_2$ nanosheets with expanded interlayer spacing for enhanced sodium storage. Inorg Chem Front. 2018;5:3099.

47. Eftekhari A. Tungsten dichalcogenides ($WS_2$, $WSe_2$, and $WTe_2$): materials chemistry and applications. J Mater Chem A. 2017;5:18299.

48. Fan S, Zou X, Du H, Gan L, Xu C, Lv W, He Y-B, Yang Q-H, Kang F, Li J. Theoretical Investigation of the Intercalation Chemistry of Lithium/Sodium Ions in Transition Metal Dichalcogenides. J Phys Chem C. 2017;121:13599.

49. Zhang R, Bao J, Pan Y, Sun CF. Highly reversible potassium-ion intercalation in tungsten disulfide. Chem Sci. 2019;10:2604.

50. Wu Y, Xu Y, Li Y, Lyu P, Wen J, Zhang C, Zhou M, Fang Y, Zhao H, Kaiser U, Lei Y. Unexpected intercalation-dominated potassium storage in $WS_2$ as a potassium-ion battery anode. Nano Res. 2019;12:2997.

51. Geng S, Zhou T, Jia M, Shen X, Gao P, Tian S, Zhou P, Liu B, Zhou J, Zhuo S, Li F. Carbon-coated $WS_2$ nanosheets supported on carbon nanofibers for high-rate potassium-ion capacitors. Energy & Environmental Sci. 2021;14:3184.

52. Mu Z, Gao S, Huo S, Zhao K. Mixed-phase 1T/2H-$WS_2$ nanosheets on N-doped multichannel carbon nanofiber as current collector-integrated electrode for potassium battery anode. J Colloid Interface Sci. 2023;630:823.

53. Lei Z, Zheng J, He X, Wang Y, Yang X, Xiao F, Xue H, Xiong P, Wei M, Chen Q, Qian Q, Zeng L. Defect-rich $WS_2$–SPAN nanofibers for sodium/potassium-ion batteries: ultralong lifespans and wide-temperature workability. Inorg Chem Front. 2023;10:1187.

54. Zhu Q, Li W, Wu J, Tian N, Li Y, Yang J, Liu B, Jiang J. Vacancy engineering in $WS_2$ nanosheets for enhanced potassium-ion storage. J Power Sources. 2022;542:231791.

55. Zhu Q, Li W, Wu J, Tian N, Li Y, Yang J, Liu B. Filling Selenium into Sulfur Vacancies in Ultrathin Tungsten Sulfide Nanosheets for Superior Potassium Storage. ACS Appl Mater Interfaces. 2022;14:51994.

56. Li Z, Yuan F, Han M, Yu J. Fast K-Ion Storage Enabled by N, O Co-Doping and Atomic-Interface Engineering on $WS_2$. Chem Eng J. 2022;450:138451.

57. Zhang Z, Yang M, Zhao N, Wang L, Li Y. Two-dimensional transition metal dichalcogenides as promising anodes for potassium ion batteries from first-principles prediction. Phys Chem Chem Phys. 2019;21:23441.

58. Jiao X, Liu X, Wang B, Wang G, Wang X, Wang H. A controllable strategy for the self-assembly of WM nanocrystals/nitrogen-doped porous carbon superstructures (M = O, C, P, S, and Se) for sodium and potassium storage. J Mater Chem A. 2020;8:2047.

59. Kang B, Chen X, Zeng L, Luo F, Li X, Xu L, Yang MQ, Chen Q, Wei M, Qian Q. In situ fabrication of ultrathin few-layered $WSe_2$ anchored on N, P dual-doped carbon by bioreactor for half/full sodium/potassium-ion batteries with ultralong cycling lifespan. J Colloid Interface Sci. 2020;574:217.

60. Xing L, Han K, Liu Q, Liu Z, Chu J, Zhang L, Ma X, Bao Y, Li P, Wang W. Hierarchical two-atom-layered $WSe_2$/C ultrathin crumpled nanosheets assemblies: Engineering the interlayer spacing boosts potassium-ion storage. Energy Storage Mater. 2021;36:309.

61. Chen X, Muheiyati H, Sun X, Zhou P, Wang P, Ding X, Qian Y, Xu L. Rational Design of Tungsten Selenide@N-Doped Carbon Nanotube for High-Stable Potassium-Ion Batteries. Small. 2022;18:2104363.

62. Zhao Z, Xu T, Yu X. Unlock the Potassium Storage Behavior of Single-Phased Tungsten Selenide Nanorods via Large Cation Insertion. Adv Mater. 2023;35:2208096.

63. Soares DM, Singh G. Superior electrochemical performance of layered $WTe_2$ as potassium-ion battery electrode. Nanotechnol. 2020;31:455406.

64. Soares DM, Singh G. Weyl semimetal orthorhombic Td-$WTe_2$ as an electrode material for sodium- and potassium-ion batteries. Nanotechnol. 2021;32:505402.

65. Li D, Sun Q, Zhang Y, Chen L, Wang Z, Liang Z, Si P, Ci L. Surface-Confined $SnS_2$@C@rGO as High-Performance Anode Materials for Sodium- and Potassium-Ion Batteries. ChemSusChem. 2019;12:2689.

66. Sun Q, Li D, Dai L, Liang Z, Ci L. Structural Engineering of $SnS_2$ Encapsulated in Carbon Nanoboxes for High-Performance Sodium/Potassium-Ion Batteries Anodes. Small. 2020;16:2005023.

67. Tan H, Feng Y, Rui X, Yu Y, Huang S. Metal Chalcogenides: Paving the Way for High-Performance Sodium/Potassium-Ion Batteries. Small Methods. 2019;4:1900563.

68. Zhou J, Liu Y, Zhang S, Zhou T, Guo Z. Metal chalcogenides for potassium storage. InfoMat. 2020;2:437.

69. Yao Q, Zhu C. Advanced Post-Potassium-Ion Batteries as Emerging Potassium-Based Alternatives for Energy Storage. Adv Funct Mater. 2020;30:2005209.

70. Wang F, Han F, He Y, Zhang J, Wu H, Tao J, Zhang C, Zhang F, Liu J. Unraveling the Voltage Failure Mechanism in Metal Sulfide Anodes for Sodium Storage and Improving Their Long Cycle Life by Sulfur-Doped Carbon Protection. Adv Funct Mater. 2020;31:2007266.

71. Cao L, Luo B, Xu B, Zhang J, Wang C, Xiao Z, Li S, Li Y, Zhang B, Zou G, Hou H, Ou X, Ji X. Stabilizing Intermediate Phases via Efficient Entrapment Effects of Layered $VS_4$/SnS@C Heterostructure for Ultralong Lifespan Potassium-Ion Batteries. Adv Funct Mater. 2021;31:2103802.

72. Yang G, Wu Y, Fu Q, Zhao H, Lei Y. Nanostructured metal selenides as anodes for potassium-ion batteries. Sustain Energy & Fuels. 2022;6:2087.

73. Wei X, Wang X, Tan X, An Q, Mai L. Nanostructured Conversion-Type Negative Electrode Materials for Low-Cost and High-Performance Sodium-Ion Batteries. Adv Funct Mater. 2018;28:1804458.

74. Liu H, Su D, Wang G, Qiao SZ. An ordered mesoporous $WS_2$ anode material with superior electrochemical performance for lithium ion batteries. J Mater Chem. 2012;22:17437.

75. Liu Y, Zhang N, Kang H, Shang M, Jiao L, Chen J. $WS_2$ Nanowires as a High-Performance Anode for Sodium-Ion Batteries. Chem. Eur. J. 2015;21:11878.

76. Srinivaas M, Wu C-Y, Duh J-G, Wu JM. Highly Rich 1T Metallic Phase of Few-Layered $WS_2$ Nanoflowers for Enhanced Storage of Lithium-Ion Batteries. ACS Sustain Chem Eng. 2019;7:10363.

77. Chen R, Li S, Liu J, Li Y, Ma F, Liang J, Chen X, Miao Z, Han J, Wang T, Li Q. Hierarchical Cu doped SnSe nanoclusters as high-performance anode for sodium-ion batteries. Electrochimica Acta. 2018;282:973.

78. Han G, Chen Z-G, Ye D, Yang L, Wang L, Drennan J, Zou J. In-doped $Bi_2Se_3$ hierarchical nanostructures as anode materials for Li-ion batteries. J Mater Chem A. 2014;2:7109.

79. Zou Z, Wang X, Huang J, Wu Z, Gao F. An Fe-doped nickel selenide nanorod/nanosheet hierarchical array for efficient overall water splitting. J Mater Chem A. 2019;7:2233.

80. He H, Huang D, Gan Q, Hao J, Liu S, Wu Z, Pang WK, Johannessen B, Tang Y, Luo JL, Wang H, Guo Z. Anion Vacancies Regulating Endows MoSSe with Fast and Stable Potassium Ion Storage. ACS Nano. 2019;13:11843.

81. Xiong P, Wu Y, Liu Y, Ma R, Sasaki T, Wang X, Zhu J. Two-dimensional organic–inorganic superlattice-like heterostructures for energy storage applications. Energy Environ Science. 2020;13:4834.

82. Dong Y, Xu Y, Li W, Fu Q, Wu M, Manske E, Kroger J, Lei Y. Insights into the Crystallinity of Layer-Structured Transition Metal Dichalcogenides on Potassium Ion Battery Performance: A Case Study of Molybdenum Disulfide. Small. 2019;15:1900497.

83. Zhang C, Wang F, Han F, Wu H, Zhang F, Zhang G, Liu J. Improved Electrochemical Performance of Sodium/Potassium-Ion Batteries in Ether-Based Electrolyte: Cases Study of $MoS_2$@C and $Fe_7S_8$@C Anodes. Adv Mater Interfaces. 2020;7:2000486.

84. Hu M, Ju Z, Bai Z, Yu K, Fang Z, Lv R, Yu G. Revealing the Critical Factor in Metal Sulfide Anode Performance in Sodium-Ion Batteries: An Investigation of Polysulfide Shuttling Issues. Small Methods. 2019;4:1900673.

85. Xiao N, McCulloch WD, Wu Y. Reversible Dendrite-Free Potassium Plating and Stripping Electrochemistry for Potassium Secondary Batteries. J Am Chem Soc. 2017;139:9475.

86. Bhide A, Hofmann J, Durr AK, Janek J, Adelhelm P. Electrochemical stability of non-aqueous electrolytes for sodium-ion batteries and their compatibility with $Na_{0.7}CoO_2$. Phys Chem Chem Phys. 2014;16:1987.

87. Hu Z, Zhu Z, Cheng F, Zhang K, Wang J, Chen C, Chen J. Pyrite FeS2for high-rate and long-life rechargeable sodium batteries. Energy Environ Sci. 2015;8:1309.

88. Li S, Zhang W, Zheng J, Lv M, Song H, Du L. Inhibition of Polysulfide Shuttles in Li–S Batteries: Modified Separators and Solid-State Electrolytes. Adv Energy Mater. 2020;11:2000779.

89. Yang X, Li X, Adair K, Zhang H, Sun X. Structural Design of Lithium–Sulfur Batteries: From Fundamental Research to Practical Application. Electrochem Energy Rev. 2018;1:239.

90. Zhang S, Ueno K, Dokko K, Watanabe M. Recent Advances in Electrolytes for Lithium-Sulfur Batteries. Adv Energy Mater. 2015;5:1500117.

91. Wang W, Bao J, Sun, C. Liquid-phase Exfoliated $WS_2$-Graphene Composite Anodes for Potassium-ion Batteries. Chinese J Struct Chem. 2020;39:493.

92. Ghosh S, Qi Z, Wang H, Martha SK, Pol VG. $WS_2$ anode in Na and K-ion battery: Effect of upper cut-off potential on electrochemical performance. Electrochimica Acta. 2021;383.

93. Chen M, Zhao J, Sun C. High-volumetric-capacity $WSe_2$ Anode for Potassium-ion Batteries. Chinese J Struct Chem. 2020;40:926.

94. Liu Y-R, Lei Z-W, Liu R-P, Li X-Y, Xiong P-X, Luo Y-J, Chen Q-H, Wei M-D, Zeng L-X, Qian Q-R. Sn-doped induced stable 1T-$WSe_2$ nanosheets entrenched on N-doped carbon with extraordinary half/full sodium/potassium storage performance. Rare Metals. 2023;42:1557.

95. Yu L, He X, Peng B, Wang W, Wan G, Ma X, Zeng S, Zhang G. Constructing ion diffusion highway in strongly coupled $WSe_2$-carbon hybrids enables superior energy storage performance. Matter. 2023;6:1604.